Int. J. Solids Structures Vol. 18, No. 11, pp. 957–973, 1982
Printed in Great Britain.

0020-7683/82/110957-17$03.00/0
Pergamon Press Ltd.

RESPONSE AND STABILITY OF ELASTOPLASTIC CIRCULAR PIPES UNDER COMBINED BENDING AND EXTERNAL PRESSURE

S. KYRIAKIDES and P. K. SHAW

Department of Aerospace Engineering and Engineering Mechanics, The University of Texas at Austin, Austin, TX 78712, U.S.A.

(*Received* 18 *September* 1981; *in revised form* 7 *January* 1982)

Abstract—The response and stability of elastoplastic circular pipes under combined bending and external pressure are investigated both analytically as well as experimentally. A virtual work approach is used to formulate the problem, which results in a set of nonlinear algebraic equations which are solved numerically. The maximum moment and curvature for different pressures are determined as a function of the material and geometric parameters of the problem. For the range of parameters where limit load instability dominates, the results compare very well with experimental results for both steel and aluminium pipes.

NOTATION

a_n, b_n, c_n, d_n	displacement coefficients
D	tube mean diameter
E	Young's Modulus
E_s	secant modulus
k	number of integration points in θ direction
l	number of integration points in z direction
M	bending moment
M_m^e	elastic limit moment
N	number of terms in series expansions
n	strain hardening parameter
P	pressure
P_c	buckling pressure
R	tube radius ($=D/2$)
t	tube thickness
U	strain energy
V	potential energy
W	work done
u, v, w	displacements
x	axial coordinate
z	distance from tube midsurface
ϵ	strain
$\epsilon_x, \epsilon_\theta$	strains in x, θ directions
$\epsilon_x^0, \epsilon_x^0$	midsurface strains
ζ	distance from cross section neutral axis
θ	circumferential coordinate
κ	curvature of tube
κ_m^e	elastic limit curvature
κ_θ	curvature in θ direction
ν	Poisson's ratio
ν_s	inelastic Poisson's ratio
σ	stress
σ_e	equivalent stress
σ_m^e	stress at elastic limit load $[=0.367(E/\sqrt{(1-\nu^2)})(t/R)]$
σ_0	yield stress
σ_x, σ_θ	stresses in x, θ direction

INTRODUCTION

The response and stability of long circular tubes under pure bending was first analyzed by Brazier [1] in 1927. He pointed out that due to ovalization of the cross section, a limit point type of instability develops which bounds the maximum allowable applied bending moment. More

precise formulation of the same problem by Reissner and Weinitschke [2, 3] yielded small differences from the Brazier solution. Kogakusi [4] extended Brazier's work to the case of combined bending and external pressure and verified the well known empirical interaction expression

$$\left(\frac{M}{M_m^e}\right)^2 + \left(\frac{P}{P_c}\right) = 1. \tag{1}$$

As has been shown by many investigators [5–9] a bifurcation type of failure can many times also occur before the limit load is reached. For short elastic cylinders this approaches the buckling stress of cylindrical shells under axial compression. For longer cylinders the critical value is much closer to the one obtained by the Brazier analysis due to the Brazier effect (ovalling of cross section).

Modern engineering applications such as offshore pipelines, risers, platforms, landbased pipelines, breeder reactor tubular components, etc., all have diameter to thickness ratios $15 < D/t < 80$. In such cases plastic effects can not be neglected. Both bifurcation as well as limit load failures are again possible. Ades [10] was able to obtain the limit point of elastoplastic long tubes in pure bending by assuming that the cross section ovalized always into an elliptical cross section. More recently Refs. [11] and [12] dealt with variations of the same problem. Gellin [13] presented an elegant solution to the limit load problem and quoted results indicating that bifurcation can sometimes occur. The difference between the results obtained from the bifurcation analysis and those obtained from the limit load analysis is more pronounced in the case of the critical curvature than for the critical moment.

In many engineering applications, like those mentioned above, long circular cylindrical pipes are acted upon by both bending and pressure. This paper presents a numerical solution for the response of elastoplastic pipes under the action of combined bending and pressure. The solution method is similar to that of Ref. [13] with noted differences in the kinematics as well as in the solution algorithm. Deformation plasticity theory is used to accomodate the inelastic material behavior. The principle of virtual work is used to derive the necessary equilibrium equations. Interaction stability boundaries based on the limit point are developed and their parametric dependence is examined. Experimental results for combined load experiments are briefly described (see Ref. [14] for more details) and compared with the numerical results.

FORMULATION OF THE PROBLEM

(a) *Kinematics*

Consider a long circular tube of mean radius R and thickness t acted upon by a uniform bending moment M and external pressure P. Let the resultant curvature be κ (Fig. 1). The displacements in the axial, circumferential and radial directions are u, v and w respectively.

First consider deformations of the pipe cross section (Fig. 2). The strains will be assumed to be small and an intermediate class of deformations will be considered such that the centroidal surface of the cross section remains inextensional. In addition, the usual assumption that normals to the centroidal axis remain normal will be adopted. The circumferential strain of the deformed cross section can be expressed as

$$\epsilon_\theta = \epsilon_\theta^0 + z\kappa_\theta, \tag{2}$$

where ϵ_θ^0 and κ_θ can be shown to be [15]:

$$\epsilon_\theta^0 = \left(\frac{v' + w}{R}\right) + \frac{1}{2}\left(\frac{v' + w}{R}\right)^2 + \frac{1}{2}\left(\frac{v - w'}{R}\right)^2 \dagger,$$

$$\kappa_\theta = \frac{1}{R}\left(\frac{v' - w''}{R}\right) \Big/ \sqrt{\left(1 - \left(\frac{v - w'}{R}\right)^2\right)}.$$

† $( )' = ( )_{,\theta}$

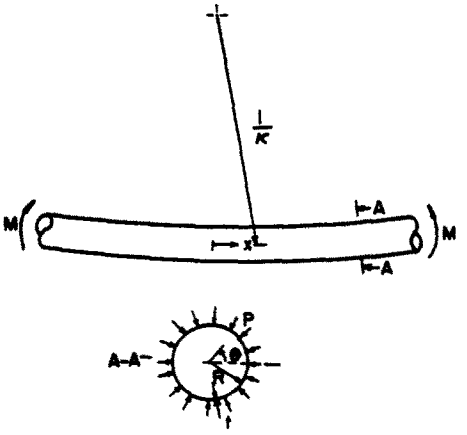

Fig. 1. Problem geometry.

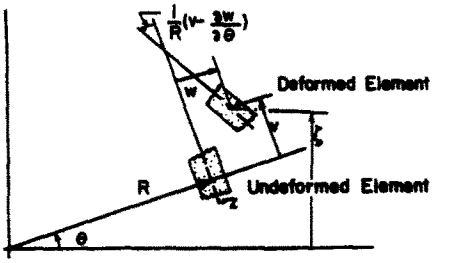

Fig. 2. Circumferential element before and after deformation.

For small strains and small rotations

$$\epsilon_\theta^0 \simeq \left(\frac{v'+w}{R}\right)+\frac{1}{2}\left(\frac{v-w'}{R}\right)^2,$$

$$\kappa_\theta \simeq \frac{1}{R}\left(\frac{v'-w''}{R}\right). \tag{3}$$

Inextensionality of the centroidal surface then requires that

$$\left(\frac{v'+w}{R}\right)+\frac{1}{2}\left(\frac{v-w'}{R}\right)^2 = 0. \tag{4}$$

Variations of the longitudinal strain through the thickness will be neglected, thus

$$\epsilon_x \simeq \epsilon_x^0(\theta) = -\zeta(\theta)\kappa. \tag{5}$$

Again, plane surfaces normal to the tube axis remain plane and normal during deformation. From geometry,

$$\zeta = [(R+w)\sin\theta + v\cos\theta]$$

and

$$\epsilon_x = -[(R+w)\sin\theta + v\cos\theta]\kappa. \tag{6}$$

(b) *Constitutive behaviour*

Due to the proportional (approximately) nature of the stresses in the problem, the deformation theory of plasticity will be used to simplify the solution considerably. For the plane stress case, the stress-strain relations reduce to

$$\sigma_x = \frac{E_s}{1-\nu_s^2}[\epsilon_x + \nu_s\epsilon_\theta],$$

$$\sigma_\theta = \frac{E_s}{1-\nu_s^2}[\epsilon_\theta + \nu_s\epsilon_x], \tag{7}$$

where E_s is the secand modulus and $\nu_s = (1/2)+(E_s/E)(\nu-1/2)$.

Experimental stress–strain curves have been approximated using the Ramberg–Osgood

relation given by

$$\epsilon = \frac{\sigma}{E}\left[1 + \frac{3}{7}\left(\frac{\sigma}{\sigma_0}\right)^{n-1}\right]. \tag{8}$$

For plane stress state, (8) leads to

$$\frac{1}{E_s} = \frac{1}{E}\left[1 + \frac{3}{7}\left(\frac{\sigma_e}{\sigma_0}\right)^{n-1}\right], \tag{9}$$

where σ_e, the equivalent stress, is given by

$$\sigma_e^2 = [\sigma_x^2 - \sigma_x\sigma_\theta + \sigma_\theta^2]. \tag{10}$$

(2), (5) and (7) give

$$\sigma_x = \frac{E_s}{1-\nu_s^2}[\epsilon_x^0 + \nu_s(\epsilon_\theta^0 + z\kappa_\theta)],$$

$$\sigma_\theta = \frac{E_s}{1-\nu_s^2}[\epsilon_\theta^0 + z\kappa_\theta + \nu_s\epsilon_x^0].$$

From St. Venant's theory of bending, ϵ_θ^0 due to bending is given by

$$\epsilon_\theta^0 = -\nu_s\epsilon_x^0$$

thus

$$\sigma_x = E_s\epsilon_x^0 + z\frac{E_s\nu_s}{1-\nu_s^2}\kappa_\theta,$$

$$\sigma_\theta = z\frac{E_s}{1-\nu_s^2}\kappa_\theta. \tag{11}$$

(c) *Principle of virtual work*

The problem to be solved is as follows. For a given tube geometry, specified by the radius R and thickness t, and for a given material specified by E, σ_0 and n, let the curvature κ and pressure P be prescribed; it is required to find the moment needed to keep it in equilibrium. The principle of virtual work in a Rayleigh–Ritz like procedure will be used to solve the problem. From the principle of virtual work, the equilibrium position is given by

$$\delta V = \delta U - \delta W = 0$$

where

$$\delta U = \int_V \sigma_{ij}\delta\epsilon_{ij}\,\mathrm{d}V = R\int_0^{2\pi}\int_{-t/2}^{t/2}(\sigma_x\delta\epsilon_x + \sigma_\theta\delta\epsilon_\theta)\,\mathrm{d}z\,\mathrm{d}\theta$$

$$= R\int_0^{2\pi}\int_{-t/2}^{t/2}\left[E_s\epsilon_x^0\delta\epsilon_x^0 + \frac{E_s}{1-\nu_s^2}z^2\kappa_\theta\delta\kappa_\theta\right]\mathrm{d}z\,\mathrm{d}\theta\dagger \tag{12}$$

and

$$\delta W = -\delta\left\{PR\int_0^{2\pi}\left[w + \frac{1}{2R}(v^2 - 2vw' + w^2)\right]\mathrm{d}\theta\right\}\ddagger$$

$$= -PR\int_0^{2\pi}\left[\left(1 + \frac{w}{R}\right)\delta w + \left(\frac{v - w'}{R}\right)\delta v - \frac{v}{R}\delta w'\right]\mathrm{d}\theta. \tag{13}$$

†This expression for δU is in agreement with the Ades[10] formulation but with $\nu_s = (1/2) + (E_s/E)(\nu - 1/2)$ instead of $\nu_s = (1/2)$.

‡See Ref. [15] for derivation.

δU and δW represent the change in strain energy and work done by the external pressure, per unit length of the deformed tube.

NUMERICAL SOLUTION

The deformation of the tube cross section is assumed to be doubly symmetric and the displacements v and w are approximated by

$$w = R\sum_{n=0}^{N} a_n \cos 2n\theta, \qquad v = R\sum_{n=1}^{N} b_n \sin 2n\theta. \tag{14}$$

For algebraic convenience let

$$\left(\frac{v'+w}{R}\right) = \sum_{n=0}^{N} c_n \cos 2n\theta \;\&\; \left(\frac{v-w'}{R}\right) = \sum_{n=1}^{N} d_n \sin 2n\theta, \tag{15}$$

thus

$$a_n = \frac{2nd_n - c_n}{4n^2-1} \text{ and } b_n = \frac{2nc_n - d_n}{4n^2-1}.$$

Substituting (15) in the inextensionality condition (4), c_n can be expressed as

$$\begin{aligned}
c_0 &= -\frac{1}{4}\left(\sum_{n=1}^{N} d_n^2\right),\\
c_1 &= -\frac{1}{2}\left(\sum_{n=1}^{N-1} d_n d_{n+1}\right),\\
&\vdots\\
c_i &= -\frac{1}{2}\left(\sum_{n=1}^{N-i} d_n d_{n+i}\right) + \frac{1}{4}\left(\sum_{n=1}^{i-1} d_n d_{i-n}\right)\\
&\vdots\\
c_N &= \frac{1}{4}\left(\sum_{n=1}^{N-1} d_n d_{N-n}\right)
\end{aligned} \tag{16}$$

where terms higher than N are truncated. From (3), (5), and (15)

$$\kappa_\theta = \frac{1}{R}\sum_{n=1}^{N} 2nd_n \cos 2n\theta$$

and

$$\epsilon_x^0 = -\kappa R\left[(1+c_0)\sin\theta + \sum_{n=1}^{N}\left[\alpha_n(\theta)d_n + \beta_n(\theta)c_n\right]\right] \tag{17}$$

where

$$\alpha_n(\theta) = \frac{1}{4n^2-1}(2n\sin\theta\cos 2n\theta - \sin 2n\theta\cos\theta)$$

and

$$\beta_n(\theta) = \frac{1}{4n^2-1}(2n\cos\theta\sin 2n\theta - \sin\theta\cos 2n\theta).$$

From (12), (13), (14), (15) and (17)

$$\sum_{i=1}^{N}\left\{\int_0^{\pi/2}\int_{-t/2}^{t/2}\left\{\kappa^2R^2E_s\left[(1+c_0)\sin\theta+\sum_{n=1}^{N}\alpha_n(\theta)d_n+\beta_n(\theta)c_n\right]\left[\alpha_i(\theta)-\frac{1}{2}d_i\sin\theta\right.\right.\right.$$

$$\left.\left.+\sum_{n=1}^{N}\beta_n(\theta)\frac{\partial c_n}{\partial d_i}\right]+\frac{E_sz^2}{1-\nu_s^2}\frac{1}{R^2}\left[\sum_{n=1}^{N}2nd_n\cos 2n\theta\right]2i\cos 2i\theta\right\}\mathrm{d}z\,\mathrm{d}\theta$$

$$\left.+PR^2\pi\left\{-(1+c_0)d_i+\frac{2ic_i-d_i}{4i^2-1}+\sum_{n=1}^{N}\frac{2nd_n-c_n}{4n^2-1}\frac{\partial c_n}{\partial d_i}\right\}\right\}\delta d_i=0. \tag{18}$$

Integration over θ and z is carried out numerically using Gaussian Quadrature. The domain is divided into k by l integration points in the θ and z directions respectively (see Fig. 3). A rule of thumb has been to keep $k > N$. The results were not very sensitive to the value of l. After integration (18) reduce to

$$\sum_{i=1}^{N}[f_i(\underline{d})-g_i(\underline{d})]\delta d_i=0;$$

thus

$$F_i(\underline{d})=f_i(\underline{d})-g_i(\underline{d})=0 \qquad i\in[1,N]. \tag{19}$$

(19) are a set of N nonlinear algebraic equations in terms of the unknown coefficient $\underline{d}$. They are solved numerically using Newton's method.

The elastic solution developed by Brazier[1] is used as the first approximation in order to start the program. Subsequently, as κ is increased the solution at κ_i is used as initial approximation for κ_{i+1}. A second Newton's method is nested in the first one in order to find values of E_s and ν_s for each new set of strains found.

After the coefficients are found the moment is calculated by integrating along the circumference the midsurface stress as follows:

$$M=Rt\int_0^{2\pi}E_s\epsilon_x\zeta\,\mathrm{d}\theta.$$

From (6)

$$M=\frac{R}{\kappa}t\int_0^{2\pi}E_s\epsilon_x^2\,\mathrm{d}\theta. \tag{20}$$

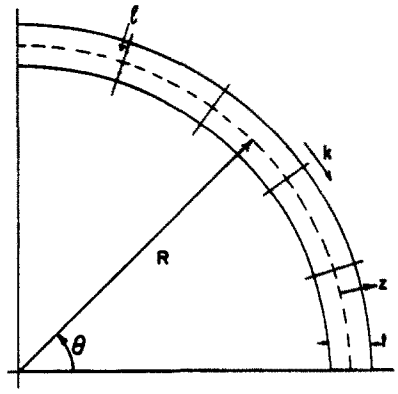

Fig. 3. Cross section quadrant with integration points.

COMBINED LOADING EXPERIMENTS

A combined bending and external pressure test facility was developed† and used to carry out a number of experiments on tubes. The facility consists of a pure bending device which slides into a pressure tank and can be operated remotely while under external pressure. Figure 4 shows a schematic representation of the bending device. It consists of two pairs of sprockets, about 9 in. (0.239 m) in diameter, symmetrically placed, about 36 in. (0.91 m) apart, on a heavy beam frame. The sprockets support two rollers which apply point loads in the form of a couple at each end of the test specimen. Heavy chains running over the sprockets are connected through a load cell and a hydraulic cylinder as shown in the figure. Rotation of the sprockets can be achieved by contracting the hydraulic cylinder. A specially designed hydraulic system is used for this purpose. The tension in the chains, measured by the load cell, is directly proportional to the applied bending moment.

The rotation of each sprocket is measured independently by a separate LVDT. The two signals are electronically added and the resultant voltage output is directly related to the curvature. (Note that this is a pure bending device so the curvature is constant along the length of the test specimen.) The specimen has freedom of movement in the axial direction due to the roller type end supports; thus no axial loads are transferred to the specimen.

The bending device was designed as a "rigid" machine, as far as the specimen is concerned. The energy absorbed by the device is less than 5% of the maximum energy stored in the deformed pipe. This type of design was chosen in order to reduce the effect the device has on the post buckling behavior of the pipe which was one of the subjects of interest in the experimental study undertaken (see Ref. [14]). The device is capable of applying moments up to 10,000 in. lb (57.1 Nm). Tubes having diameters from 0.75–1.5 in. (19–38 mm) and lengths from 25 50 in. (0.6–1.5 m) can be tested.

The bending device loaded with the test specimen slides into the pressure tank for simultaneous application of external pressure (Fig. 5). The tank has a diameter of 18 in. (0.46 m) and working pressure of 800 psi (55.2 bar). It can be pressurized by water, air or partially filled with water and pressurized by air. The bending device can be remotely controlled from outside the tank. The LVDT's, load cell and their respective wiring systems are hermetically sealed and can operate under high water pressure. A more detailed description of the test facility, its calibration as well as the experimental procedure followed, can be found in Ref. [14].

In all experiments presented, aluminum 6061-T6 tubes of nominal lengths of 29 in. (0.74 m) were used. Pressure was applied first and then the tube was gradually bent. The signals from the load cell, LVDT's and pressure transducer were recorded on a common time base. The recorded signals were easily reduced to the required moment, curvature and pressure measurements. A tube buckled under pure bending is shown in Fig. 6. It is characterized by one clear crosswise dent. The buckling deformation is restricted to a length of about 10 tube diameters. For combined loading, the damage has the same geometric characteristics but for pressures higher than the Propagation Pressure[16] of the tube, the possibility exists that a propagating buckle will occur. Such a buckle is initiated from the bending buckle and then driven by the external pressure to flatten the whole length of tube.

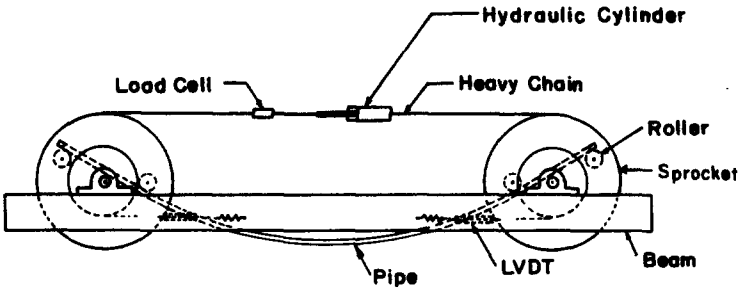

Fig. 4. Pure moment bending device.

†The facility was develop while the first author served as a Research Fellow at the California Institute of Technology.

Fig. 5. Combined bending—pressure test facility.

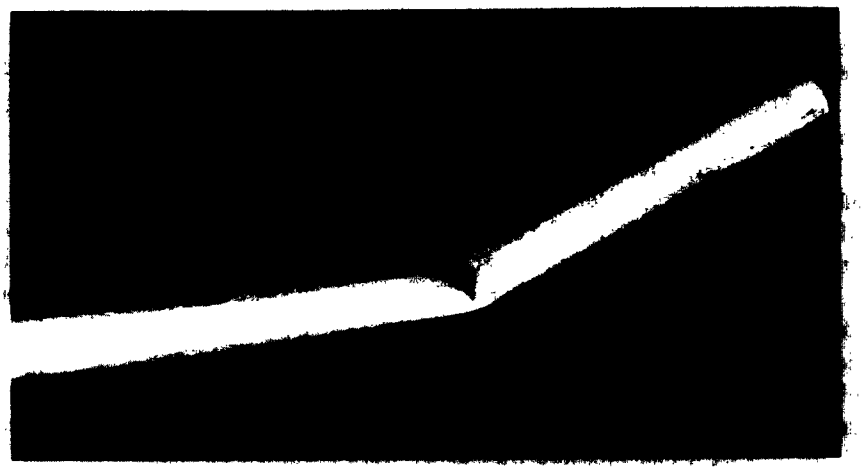

Fig. 6. Tube buckled under pure bending ($D/t = 34.71$, Al-6061-T6).

RESULTS AND DISCUSSION

(a) *Elastic case*

The linearly elastic case can be treated as a special case of the more general nonlinear inelastic case described above. The material properties become constant through the thickness. Thus E_s and ν_s are replaced with E and ν. The need of the second iteration to find E_s no longer exists. To improve the efficiency of the computation a simplified algorithm was used for the elastic case where the nested iteration was avoided and the integration through the thickness was carried out in closed form. Six integration points were taken in the θ direction (i.e. $k = 6$). After a number of tries it was found that four term expansions of the displacements (i.e. $N = 4$) produced sufficient accuracy.

The solution procedure was as follows. The curvature (κ) and pressure (P) were prescribed for each cycle. The algorithm usually converged in 3–4 iterations. The convergence criteria were $\|F_i(\underline{q}^{(n)})\| \leq 10^{-4}$. The curvature was gradually incremented each time finding the corresponding moment. This continued until the moment decreased with an increase in curvature, indicating that the limit point was passed. The curvature was then bisected and the new moment was compared with the previous largest value. This procedure was continued until an accuracy of 0.5% for the limit curvature was achieved.

Figure 7 shows the moment curvature response of an elastic tube for different values of

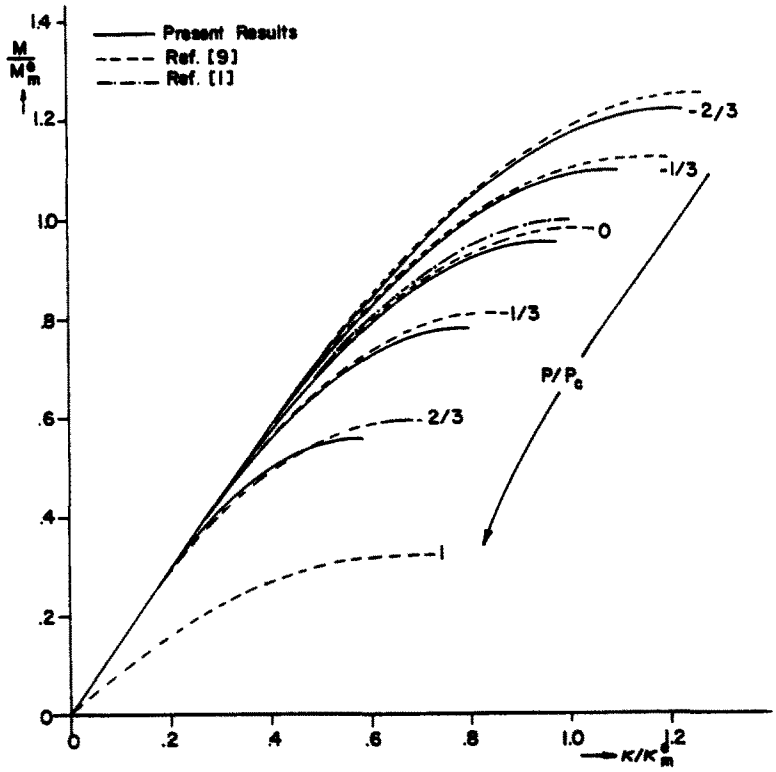

Fig. 7. Moment curvature response for different pressures (elastic case).

pressure. The moment and curvature are normalized by the limit point values obtained by Brazier[1].

i.e.
$$M_m^e = \frac{2\sqrt{2}}{9}\pi \frac{E}{\sqrt{(1-\nu^2)}} Rt^2, \tag{21}$$

and

$$\kappa_m^e = \frac{\sqrt{2}}{3}\frac{1}{\sqrt{(1-\nu^2)}}\frac{t}{R^2}. \tag{21}$$

External pressure (P) is defined as positive and is normalized by the buckling pressure (P_c) of a long elastic tube given by

$$P_c = \frac{E}{4(1-\nu^2)}\left(\frac{t}{R}\right)^3. \tag{22}$$

Brazier only considered the case of zero pressure. His results are also plotted on the same figure. At the limit point of the zero pressure case

$$\frac{M}{M_m^e} = 0.950 \text{ and } \frac{\kappa}{\kappa_m^e} = 0.957.$$

The small difference is mainly due to the more accurate representation of the strains in the present analysis through the nonlinear relation (3); it also serves as a strong reassurance as to the dependability of the Brazier solution.

The results from Fig. 4 of [9] are also plotted on the same figure. Very little difference is observed in all the results except those for high external pressure. The limit loads were

calculated for different pressures and the results are plotted in Fig. 8. Expression (1) is also included on the same plot together with the results from [9]. At low values of pressure all three sets of results are very close. For values of pressure $(P/Pc) > 0.7$ the solution of [9] deviates considerably. It should be noted that both solutions can not predict the buckling load of a tube under external pressure and zero moment. However for small values of moment this point can be approached very closely by the present solution. The results of [9] seem to imply a substantial increase in the buckling load due to the application of a small bending moment. This is intuitively unacceptable.

Again it can be concluded that provided correct values for M_m^c and P_c are known, expression (1) gives a very good approximation to the stability interaction curve. This result is independent of D/t. However it must be noted that for a range of D/t bifurcation will occur before the limit load is reached. This subject is further discussed in [9].

(b) *Inelastic case*

For the inelastic case the Ramberg–Osgood approximation for the stress-strain relationship of the material was used. Its use allows direct representation of the curve by only three parameters. This was particularly helpful in the parametric study of the limit point that was one of the objectives of this study. In addition good fit of the actual $\sigma - \epsilon$ curves of the materials used in the experiment was achieved. The $\sigma - \epsilon$ behavior was assumed to be the same in tension and compression.

As in the elastic case it was again found that a four term $(N = 4)$ series expansion of the displacements was adequate. Six integration points were taken through the thickness and six in the θ direction $(k = l = 6)$. The convergence criteria were the same as in the elastic case. The solution procedure was also the same.

The case of pure bending of thin elastoplastic tubes was treated in some detail in [13]. A number of spot checks were run and the results were compared with those of Figs. 2 and 3 of [13]. No visible difference between the two sets of results was observed. Since in the case of the above reference the exact representation for the strains ϵ_θ^0 and κ_θ^0 was used, it can be concluded that the approximations made in the present analysis by adopting versions (3) for these quantities, was justified and helped in increasing the efficiency of the algorithm.

As mentioned earlier, Ades[10] carried out a similar type of analysis for the pure bending case but he used the assumption that the cross section deforms into an ellipse. A number of

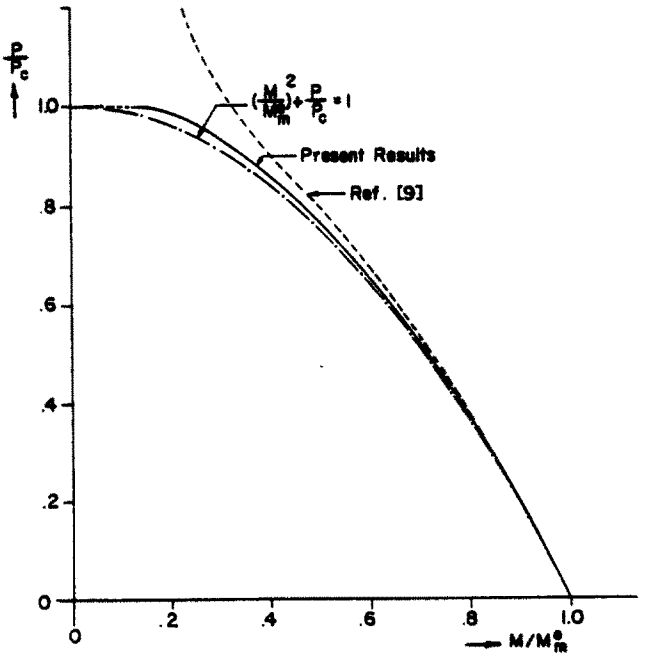

Fig. 8. Moment-pressure interaction stability diagram for elastic case.

comparative runs were made for the cases presented in Fig. 6 of [10]. The maximum difference found was less than 5%. This suggests that Ades' assumption is acceptable (at least for the range of parameters he considered).

For the case of combined loading, the pressure was prescribed and the curvature was gradually increased until the limit point was reached. At first a set of cases were run using the parameters of the tubes tested experimentally. Some representative results are shown in Fig. 9 together with the experimental results. Some difference is noticed especially in the critical moment where the experimental results are 5–10% lower than the ones predicted by theory. The limit curvature is closer to the experimental results but is again overestimated by theory. Experiments were also run where the moment was applied first followed by gradual application of the pressure until buckling occurred. No noticeable difference was observed in the two sets of results.

The limit moment normalized by the elastic limit moment (M_m^e) is plotted vs the pressure in Fig. 10. The results from 25 experiments are also included. Aluminum 6061-T6 tubes were used in all experiments. The tube nominal diameter was 1.250 in. and the thickness 0.035 in. The stress-strain curve obtained from a longitudinal specimen cut out of one of the tested tubes was fitted using the Ramberg–Osgood approximation and the parameters (listed in Fig. 10) were used as input to the algorithm.

For offshore pipeline applications the curvature is a preferred parameter because it is one of the parameters controlled in the laying operation. Due to this, the critical curvature is also plotted vs the pressure in Fig. 11 for the same parameters. The experimental results are also included in the same figure. In both cases the theoretical results overestimate those obtained from experiments. The biggest discrepancy seems to occur for higher pressures. Some scatter is also observed in the experimental results.

One factor that could generate the observed difference between experimental and theoretical results is the presence of initial imperfections in the tubes tested. These manifest themselves in the form of geometric imperfections as well as material property nonuniformities although the latter are less important. Gellin[17] showed that as in the case of an elastic material, the buckling load of an axially loaded inelastic cylindrical shell is greatly reduced by

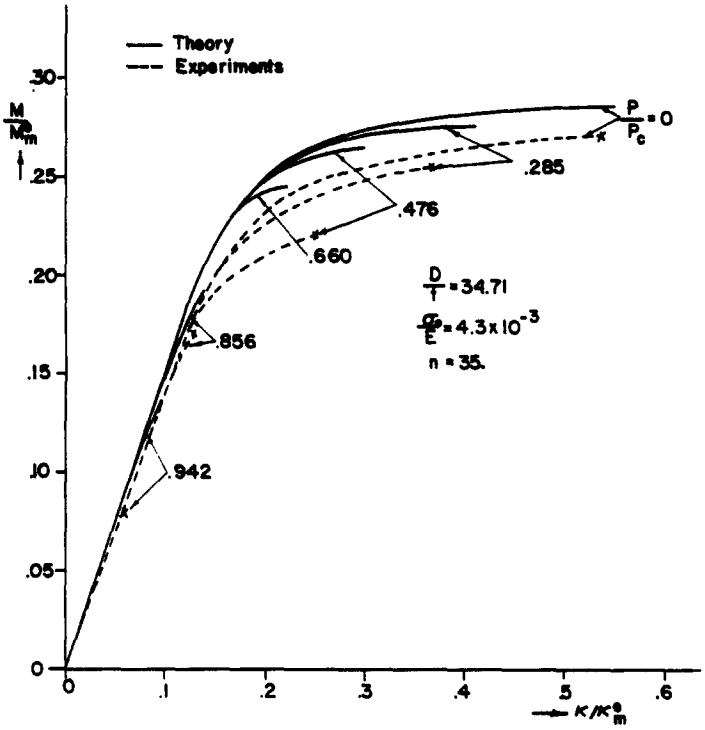

Fig. 9. Moment-curvature response for different pressures. Comparison between theory and experiments.

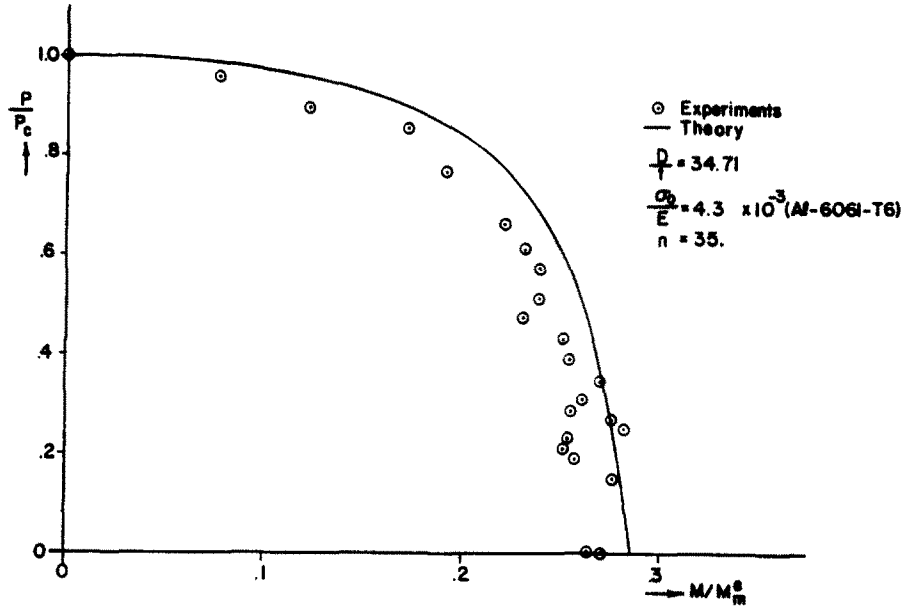

Fig. 10. Moment-pressure interaction, comparison between theory and experiments.

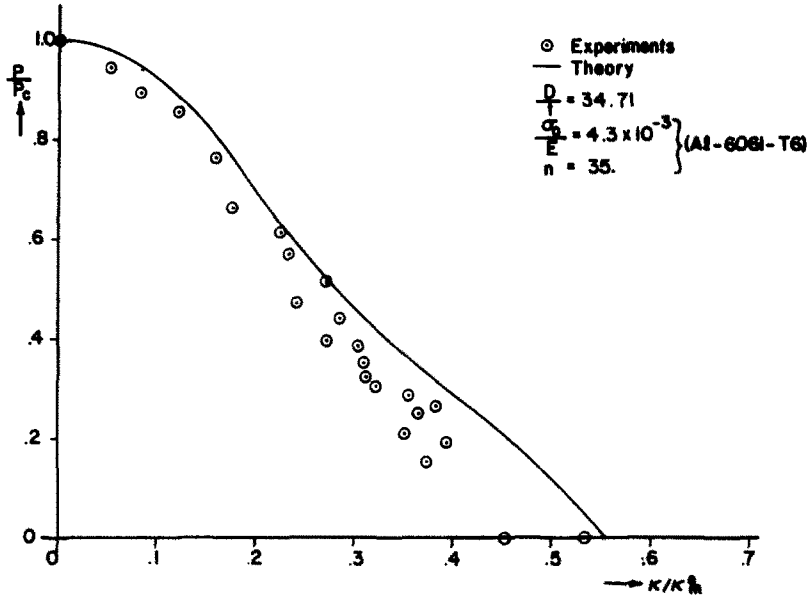

Fig. 11. Curvature-pressure interaction, comparison between theory and experiments.

the presence of initial imperfections. Their effect in the case of this problem has yet to be quantified but due to the close relationship between the two problems this is bound to be significant.

The observed scatter in the experimental results is also due to differences in both material ($E = 10^7 \pm 0.5 \times 10^7$, $\sigma_0 = 43 \times 10^3 + 5 \times 10^3$, -2×10^3) as well as the geometry (e.g. $t = 0.035 \pm 0.001$ in, $D = 1.250 \pm 0.005$ in) of the tubes tested. These variations could not be normalized out for the way the results are presented. Other sources of error such as in calibration of instruments, the exact estimation of the tube affected length in the experiments as well as the usual human errors are thought to have also contributed (but not significantly) to the observed

difference. It must be emphasized that the theoretical predictions originate from a limit load type of analysis. As mentioned earlier the possibility of bifurcation type of failure, occurring before the limit load is reached still exists. Close examination of the experimental moment curvature response at zero pressure (Fig. 9) leads to the conclusion that the tested pipe buckled at its limit load. For higher pressures the situation is not as clear. In any case, due to the nature of the response curve, premature bifurcation would not affect the critical moment by very much but would affect the critical curvature drastically. In this case the difference between the theoretically predicted results and those of the experiments is of equal magnitude for both the moment and curvature indicating that perhaps the difference is not due to premature bifurcation but due to other factors like the ones cited above. A separate analysis finding the interaction bifurcation load is necessary in order to establish when bifurcation occurs first.

Similar experiments, but using steel pipes, are also presented in Ref. [18] for $D/t = 40$, 60 and 80. Using their parameters, theoretical predictions were obtained through the present analysis. These experimental results are plotted with the theoretical predictions obtained, in Fig. 12. The comparison is very good for $D/t = 40$ and gets progressively worse for $D/t = 60$ and 80. The same reference also estimates that for such tubes bifurcation type failure dominates the behaviour for $D/t > 50$ whereas for $D/t < 50$ the limit load is reached first. This is in agreement with the comparison made in Fig. 12.

From all the above it can be concluded that the presented analysis represents a successful estimation of the limit loads of tubes under combined pressure and bending. One further measurement made experimentally was that of the change in diameter of the tube as the moment is increased. The case of pure moment is shown in Fig. 13 compared to the theoretical prediction. Although lower, the experimental results compare well with the theoretical ones. The influence of ovalization in both the elastic as well as the inelastic case must be emphasized. Ovalization is what actually leads to the observed nonlinear behaviour and eventually to the limit load type of instability. Even if bifurcation occurs first the load at bifurcation is very much affected by the nonlinear nature of the moment-curvature response in all but for very shoft tubes [5].

Having gained confidence in the presented analysis a parametric study of the interaction problem is carried out. In Fig. 14 the moment-pressure interaction stability diagrams are drawn as a function of D/t for σ_0, E and n constant. The corresponding curvature-pressure interaction

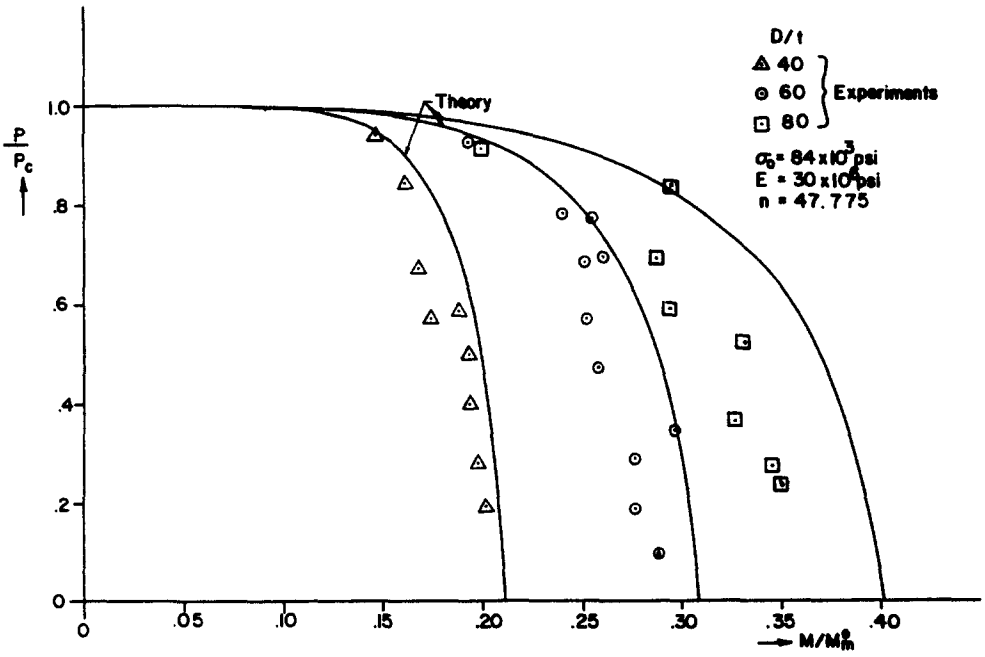

Fig. 12. Comparison between experimental and theoretical results for steel pipes.

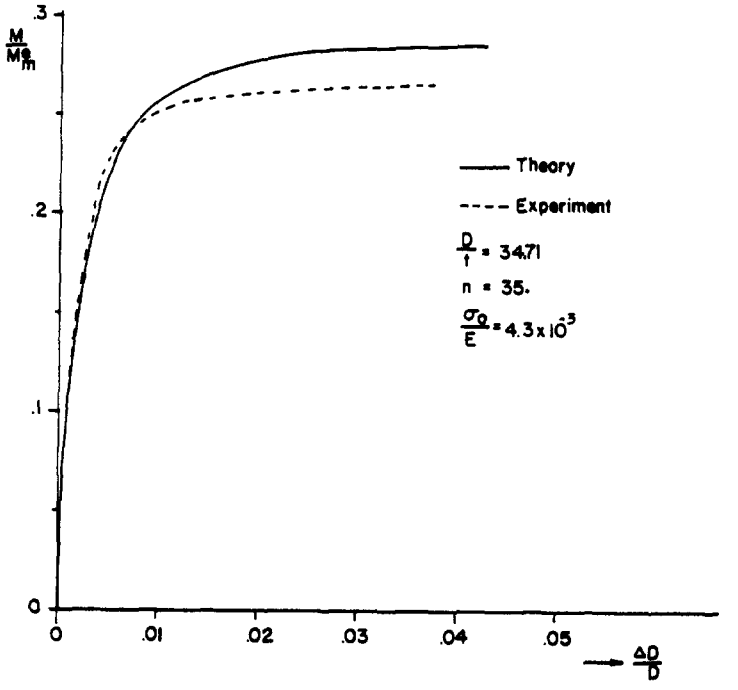

Fig. 13. Change of tube diameter during pure bending.

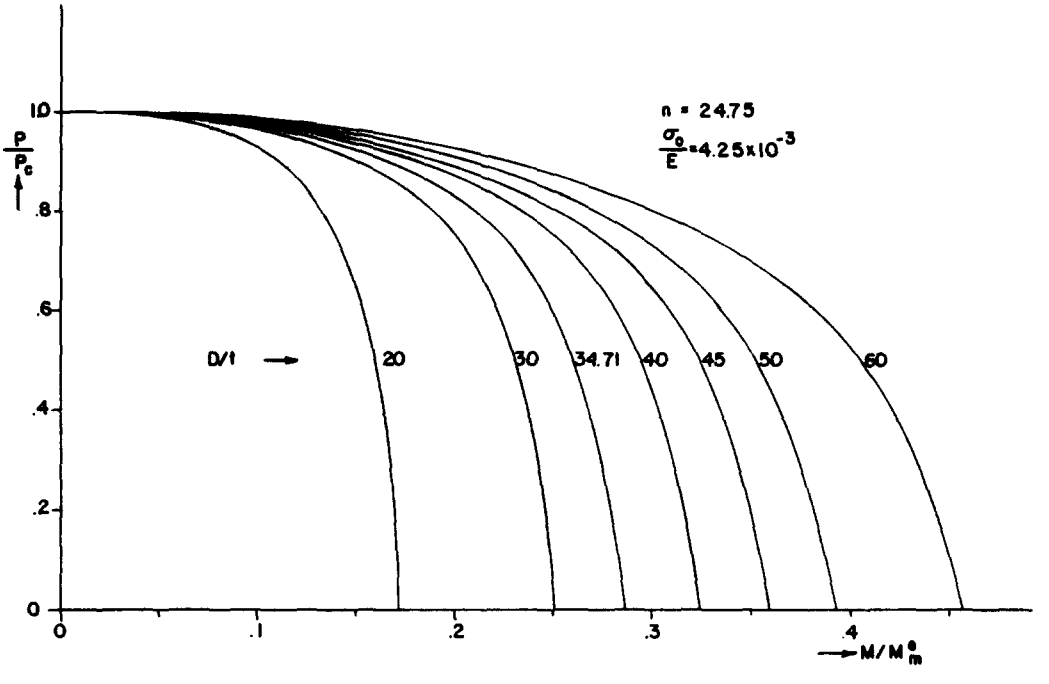

Fig. 14. Moment-pressure interaction for different D/t (inelastic case).

diagrams are presented in Fig. 15. Unlike the elastic case a strong dependence on D/t is observed in both cases. For lower D/t plastic effects force an early deviation from the elastic cases.

The yield stress is varied in Figs. 16 and 17 keeping D/t and n constant. Clearly any reduction of the yield stress drastically reduces the limit values. The strain hardening parameter n is varied in Figs. 18 and 19 with the other parameters kept constant. Its effect however is less significant than that of the yield stress.

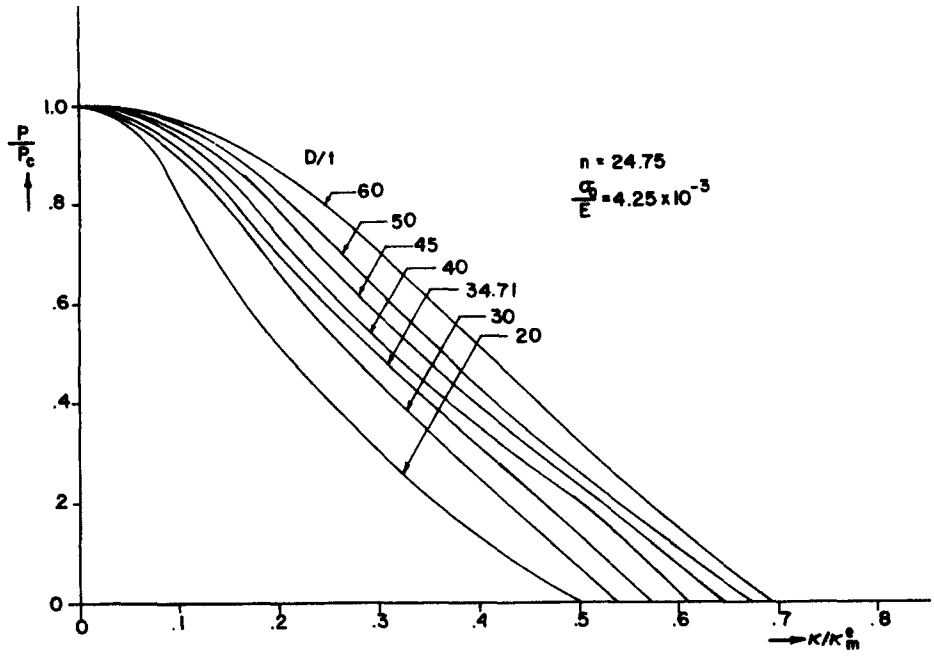

Fig. 15. Curvature-pressure interaction curve for different D/t (inelastic case).

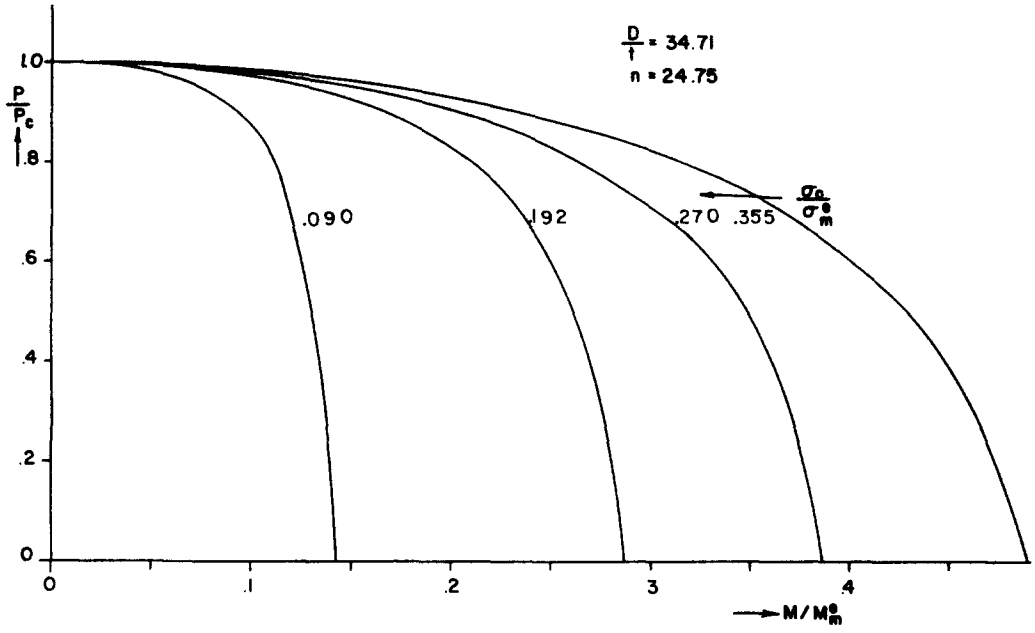

Fig. 16. Moment-pressure interaction for different σ_0/σ_m^e.

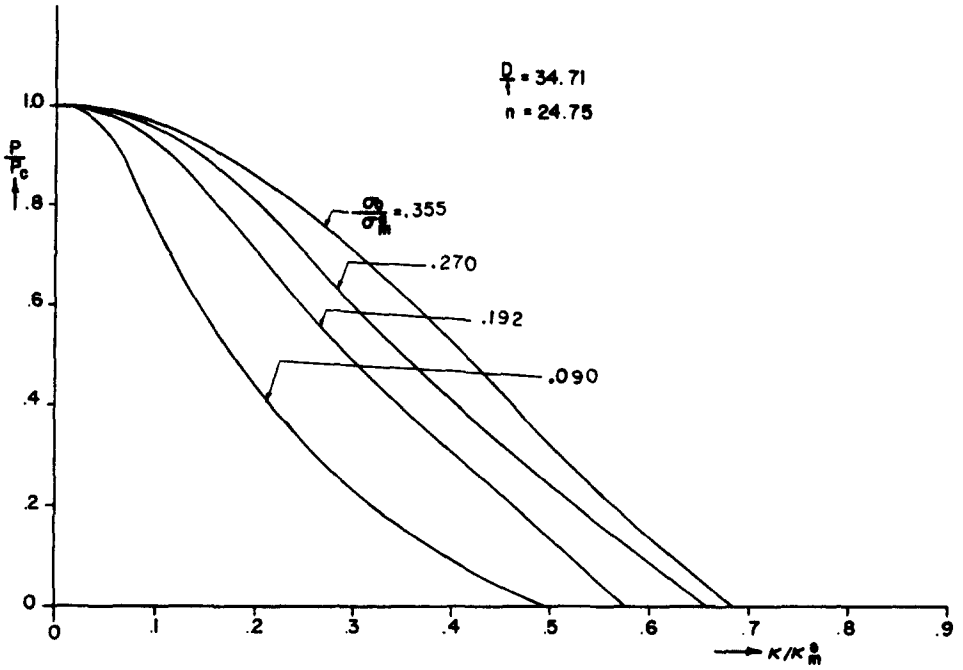

Fig. 17. Curvature-pressure interaction for different σ_0/σ_m^0.

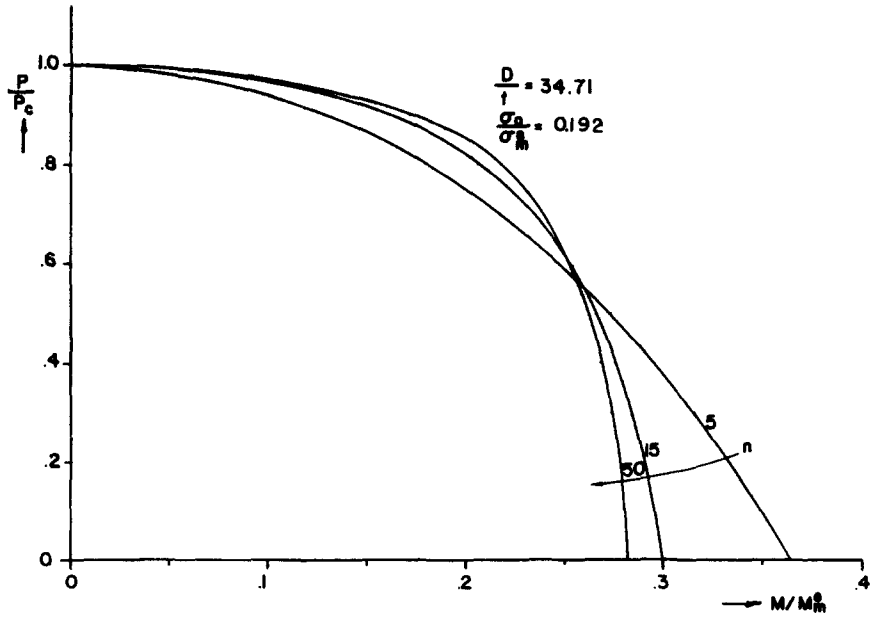

Fig. 18. Limit moment vs pressure for different n.

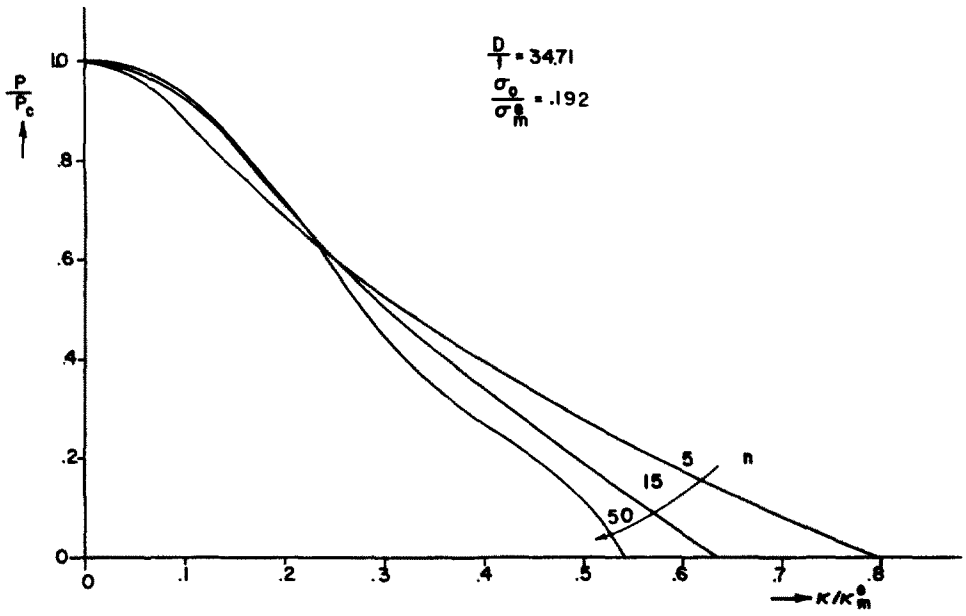

Fig. 19. Curvature-pressure interaction for different n.

Acknowledgements—The presented experimental work was carried out while the first author was a Post-Doctoral Fellow at the California Institute of Technology. This author wishes to thank Professor C. D. Babcock for his guidance and support during that period. Special thanks go to Ms. Linda Penrod for typing the manuscript. The paper was prepared with the support of the National Science Foundation under Grant CEE-8105539. Their support is gratefully acknowledged.

REFERENCES

1. L. G. Brazier, On the flexure of thin cylindrical shells and other "thin" sections. *Proc. R. Soc.* Series A, **116**, 104 (1927).
2. E. Reissner, On finite pure bending of cylindrical tubes. *Österr. Ing. Arch.*, **15**, 165 (1961).
3. E. Reissner and H. J. Weinitschke, Finite pure bending of cylindrical tubes. *Quart. Appl. Math.* **20**, 305 (1963).
4. K. I. Kogakusi, Failure of thin circular tubes under combined bending and internal or external pressure. *J. Japanese Soc. Aerospace Engineers* 7, 1109 Dec. 1940.
5. P. Seide and V. I. Weingarten, On the buckling of circular cylindrical shells under pure bending. *J. Appl. Mech.* **28**, 112 (1961).
6. W. B. Stephens, J. H. Starnes and B. O. Almroth, Collapse of long cylindrical shells under combined bending and pressure loads. *AIAA J.* **13**, 20 (1975).
7. E. L. Axelrad, Refinement of critical load analysis for the tube flexure by way of considering precritical deformation. *Izv. AN SSSR, ONT, Mech.*; *Mash.* **4**, 123 (1965) (in Russian).
8. E. L. Axelrad, Flexible shells. *Proc. 15th IUTAM*, 1980, Toronto, Canada, pp. 45–56.
9. O. Fabian, Collapse of cylindrical, elastic tubes under combined bending, pressure and axial loads. *Int. J. Solids Structures* **13**, 1257 (1977).
10. C. S. Ades, Bending strength of tubing in the plastic range. *J. Aero. Sci.* **24**, 605 (1957).
11. B. D. Reddy, An experimental study of the plastic buckling of circular cylinders in pure bending. *Int. J. Solids Structures*, **15**, 669 (1979).
12. P. Tugcu and J. Schroeder, Plastic deformation and stability of pipes exposed to external couples. *Int. J. Solids Structures* **15**, 643 (1980).
13. S. Gellin, The plastic buckling of long cylindrical shells under pure bending. *Int. J. Solids Structures* **16**, 397 (1979).
14. S. Kyriakides, On the stability of inelastic circular pipes under combined bending and external pressure. *Proc. SESA*, Spring 1981, pp. 372–378.
15. D. O. Brush and B. O. Almroth, *Buckling of Bars, Plates and Shells*, Chap. 4, pp. 120–141. McGraw-Hill, New York (1975).
16. S. Kyriakides and C. D. Babcock, Experimental determination of the propagation pressure of circular pipes. *J. Pressure Vessel Technology, Trans. ASME* **103**, 328–336 (1982).
17. S. Gellin, Effect of axisymmetric imperfections on the plastic buckling of an axially compressed cylindrical shell, *J. of Appl. Mech.* **46**(1), 125 (1979).
18. T. G. Johns, R. E. Mesloh, R. Winegardner and J. E. Sorenson, Inelastic buckling of pipelines under combined loads. *Proc. Offshore Tech. Conf.*, OTC 2209, pp. 635–646, (1975).
19. J. O. Jirsa, F. H. Lee, J. C. Wilhoit and J. E. Merwin, Ovaling of pipelines under pure bending. *Proc. Offshore Techn. Conf.* OTC 1569, pp. 573–578 (1972).